X-ray study of the ferroelectric $[Ba_{0.6}Sr_{0.4}]$ $[(YTa)_{0.03}Ti_{0.94}]O_3$

P. Shanthakumar,[1] M. Balasubramanian,[2] D. M. Pease,[1] A. I. Frenkel,[3] D. M. Potrepka,[4] V. Kraizman,[5] J. I. Budnick,[1] and W. A. Hines[1]

[1]*Department of Physics, University of Connecticut, Storrs, Connecticut 06269, USA*

[2]*Advanced Photon Source, Argonne National Laboratory, Argonne, Illinois 60439, USA*

[3]*Department of Physics, Yeshiva University, New York, New York 10016, USA*

[4]*Sensors and Electronic Devices Directorate, U.S. Army Research Laboratory, Adelphi, Maryland 20783, USA*

[5]*Rostov State University, Rostov on Don 344104, Russia*

(Received 9 June 2006; revised manuscript received 29 August 2006; published 3 November 2006)

We have studied the system $[Ba_{0.6}Sr_{0.4}]$ $[(YTa)_{0.03}Ti_{0.94}]O_3$, as produced using two different sintering temperatures. It was shown by others that for a sample sintered at 1550 °C the material is a relaxor, whereas for the same composition produced with sintering temperature of 1600 °C the sample is a normal ferroelectric. We have employed analysis of x-ray diffraction peak broadening, Ti *K* edge x ray near edge spectroscopy, and extended x-ray absorption edge fine structure spectroscopy of Ta and Y sites in our study. We find that the 1550 °C sinter sample has over double the lattice strain as does the 1600 °C sample. For the lower temperature sinter material, both Ta and *Y* go to sites substitutional for Ti in the lattice, with a significant expansion (contraction) of the local perovskite structure about Y (Ta) dopants. Thus, with only three percent *B* site addition of Y and Ta dopants, there is a strain associated relaxor behavior produced in a bulk sample. For the higher temperature sinter specimen, there is a marked change in the average Y environment relative to the lower temperature sinter sample.

DOI: 10.1103/PhysRevB.74.174103 PACS number(s): 77.84.Dy, 68.55.Ln

I. INTRODUCTION

Potrepka *et al.* have shown that charge-balanced substitutions of Y^{3+} and Ta^{5+} ions into $Ba_xSr_{(1-x)}TiO_3$ (BST) can lead to a broadening of the temperature dependence of ferroelectric properties.[1,2] Such relaxorlike[3] behavior can be desirable in applications that emphasize device tunability, such as, in capacitors of dynamical random access memory, infrared pyroelectric sensors, electro-optics, and tunable microwave devices.[4,5]

Besides high capacitance and low losses, a lessening of temperature dependence of the dielectric properties is required for many applications. Potrepka *et al.* have discovered a marked effect of changes in $[Ba_{0.6}Sr_{0.4}]$ $[(YTa)_{0.03}Ti_{0.94}]O_3$, as sintered at 1550 °C (sample *A*) versus 1600 °C (sample *B*).[1,2] In these materials, it is presumed by Potrepka *et al.* that Ta substitutes for Ti^{+4} as a Ta^{+5} ion and Y substitutes for Ti^{+4} as a Y^{+3} ion. A plot of real relative permittivity versus temperature shows a sharp peak at −60 °C for sample *B*. Such a peak is absent for *A*. Even at room temperature, for which our composition of BST is paraelectric, the relative permeability of *B* significantly exceeds that of *A* by about 50%. One way of summarizing these results would be to state that sample *A* is much more "relaxor" like than *B* if we mean by relaxor behavior that there is a "diffuseness of the temperature dependence of the various properties that relate to the polarization of the material."[3]

An illustration of a perovskite unit cell with a much exaggerated tetragonal distortion is shown in Fig. 1. At room temperature, BST is found, by x-ray diffraction (XRD), to be cubic for *x* less than 0.7.[6] Our samples have a value of *x* of 0.6 and are therefore expected to appear cubic, as verified by our XRD characterization. Despite the fact that our experiments were carried out at room temperature on paraelectric samples, we find, in agreement with other investigators, that the Ti atom location, measured *locally*, is not at the center of the surrounding oxygen octahedron, but displaced from the center. It is now well established for a number of perovskite ferroelectrics that local Ti displacements persist in the paraelectric phase, despite the fact that the *spatially averaged* structure observed by XRD is cubic.[7,8] Furthermore, there is evidence that for particle sizes less than 0.1 μm, the tetragonal distortion and ferroelectricity in cubic $BaTiO_3$ may be suppressed, even for temperatures much less than the T_C of bulk material.[9] Even for a ferroelectric sample of pure

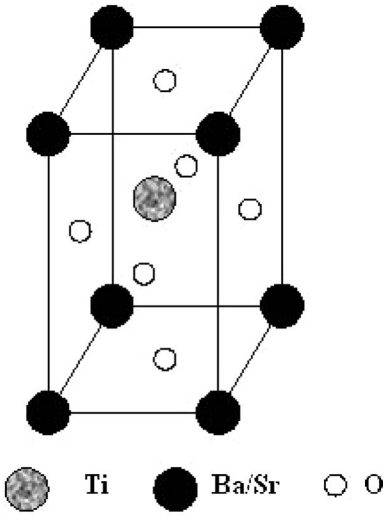

FIG. 1. Schematic illustration of perovskite structure in tetragonal phase of ferroelectric BST as inferred from x-ray diffraction. Under our conditions the average structure observed by x-ray diffraction is cubic.

 ©2006 The American Physical Society

$BaTiO_3$ at room temperature, the tetragonal distortion is found by XRD to be quite small, with a c/a ratio of only 1.01. Crowne *et al.* have modeled this Ta/Y doped BST system in terms of internal electric fields associated with nonrandom clustering of the Y^{+3} and Ta^{+5} ions.[10] In this model, charge compensation occurs at the Ti^{+4} sites where substitutional occupancy of Ta^{+5} or Y^{+3} is localized, so that clustering Ta^{+5} and Y^{+3} impurities form permanent dipoles.

Characteristic relaxor behavior is manifested as a broadening of the temperature dependence of various polarization-dependent properties. Two early models proposed to describe relaxor behavior are the composition fluctuation model of Smolenskii *et al.*[11] and the domain size effect model of Cross.[12] Smolenskii suggested that compositional fluctuations, on the nanoscale, lead to fluctuations in ferroelectric Curie temperature in disordered material.[11] In the model of Cross, one can have a situation in which the domain size is sufficiently small that the polarization direction is altered by thermal agitation.[12] The temperature at which the polarization direction can be switched back and forth by thermal energies depends on the size of the domain. Consequently, in a sample with many small domains, but of different domain sizes, there will be a suite of differing Curie temperatures, and consequently, relaxor behavior. Cross points out the analogy between this type of domain size determined ferroelectric Curie temperature and the "blocking temperature" effect observed in nanoscale ferromagnets.[12]

Subsequent to the Smolenskii and Cross models, there have been other explanations proposed for relaxor behavior. Viehland *et al.* suggest that relaxor ferroelectrics are analogous to magnetic spin glass systems, and will exhibit thermally activated polarization fluctuations above a freezing temperature.[13] Westphal *et al.* propose that relaxor behavior originates from quenched random electric fields,[14] a model that is along the lines of the treatment of $[Ba_{0.6}Sr_{0.4}][(YTa)_{0.03}Ti_{0.94}]O_3$ by Crowne *et al.* mentioned above.[10] For the present study, it is important to consider the possible effects of internal strains. A linear augmented plane wave calculation indicates that both increasing pressure and increasing temperature can transform $BaTiO_3$ from tetragonal to cubic phase. However, whereas increasing temperature destroys long range correlations between surviving atomic off center displacements, Cohen and Krakauer predict that increasing pressure destroys the local ferroelectric instability and local Ti displacements can be completely suppressed.[15]

In the present study, we have investigated the Ta, Y doped BST system by XRD peak broadening analysis, Ti *K*-edge x-ray absorption near edge spectroscopy (XANES), and Ta L_3 and Y *K*-edge extended x-ray absorption edge fine structure (EXAFS).

II. EXPERIMENTAL DETAILS

The preparation of the $[Ba_{0.6}Sr_{0.4}][(YTa)_{0.03}Ti_{0.94}]O_3$ material is described by Potrepka *et al.*[2] Starting materials of 99.9% purity or better were mixed until homogeneous, then compacted with a steel die and calcined in air at 1100 °C for 8 h. The calcined materials were then reground to powders with 75 μm or smaller grain size, pressed at 50 kpsi in an isostatic press, and sintered at the respective sinter temperature in air for 40 h. The samples were bulk ceramics during the measurements, not single crystalline. We also include samples of pure $SrTiO_3$, and undoped $Ba_{0.6}Sr_{0.4}(TiO_3)$ (BST) as part of our study. Existing data on $BaTiO_3$ and $EuTiO_3$ are used for reference. X-ray diffraction characterization is performed on all samples studied. The $SrTiO_3$, BST, and both Ta/Y doped BST samples are found to be pure cubic phase material. The diffraction peak intensities indicate no significant preferred orientation. No oxide diffraction peaks were found for either sample. We note that the ratio of Ba to Sr in our BST is just smaller than the critical concentration for the cubic to tetragonal transition at room temperature.[6]

The XAFS studies of Ti edges were performed at the X-11B beam line at the National Synchrotron Light Source (NSLS). The Si (111) reflection was used for the beam line monochromator. The Ti *K*-edge XANES were obtained in the fluorescence mode, using an ion chamber. A common problem in obtaining XAFS data for crystalline samples is due to the fact that as the incident beam energy is increased, the Ewald sphere radius increases and the sphere suddenly will intersect reciprocal lattice points during the scan. This diffraction peak problem can often be solved by sample spinning, which is a standard technique in such cases. The BST, $SrTiO_3$, and both Ta, Y doped BST samples were spun. As will be seen below, the Ti *K*-edge x-ray absorption near edge spectra (XANES) were nearly identical for the BST as for the Ta and Y doped BST corresponding to samples *A* and *B*. In addition, some data was collected for Ti edges of samples *A* and *B* without sample spinning and identical XANES was obtained as with spinning, showing that diffraction peak effects on the XAFS were not present.

For the diffraction peak width analysis, a Bragg-Brentano diffractometer was used, outfitted with a copper anode and graphite monochromator. Reference data were taken using a LaB_6 standard purchased from NIST. The Ta L_3 edges of samples *A* and *B* were obtained at the X-11B line of the NSLS, using three scans for each sample, a Si(111) monochromator, and an ion chamber with argon counter gas. The Y *K*-edges presented a special problem, in that Y is just to the right of Sr in the periodic table. Therefore, the dilute Y *K*-edge lies on top of the intense background of the Sr absorption edge. Fortunately, however, the Sr and Y edges are sufficiently separated in energy that the Sr EXAFS oscillations do not interfere with the Y signal. Under these circumstances, a method developed by Heald can be used,[16] and data was obtained, using this method, at the sector 20 PNC/XOR bending magnet beam line of the Advanced Photon Source (APS). In Heald's method, one uses a multielement energy dispersive detector. The saturation effects in the energy dispersive detector, due to the rejected Sr background, are corrected for using the following procedure: The Sr and Y fluorescence energies are separately windowed, and the fluorescence Y XAFS is normalized, not with the incident photon ion chamber signal, but with the Sr signal. Both windowed energies, for dilute Y on top of a concentrated Sr background, have the same "pile up" distortion and the distortion is therefore corrected for by normalizing with the Sr signal.

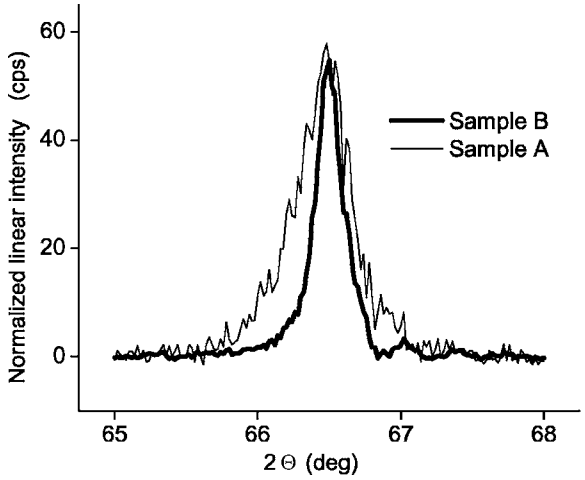

FIG. 2. XRD data obtained on samples *A* and *B*, with the $K\alpha_2$ line stripped from the data. Diffraction scans shown are in the region of the (220) reflection, using a copper anode diffractometer. The peaks are normalized to exhibit the same maximum value, for ease in visualization. Thus, the count rate shown on the ordinate scale refers to sample *B*. The broader peak of sample *A* is normalized to peak *B*.

III. EXPERIMENTAL RESULTS

A. Diffraction peak broadening analysis

We have analyzed the full width at half maximum (FWHM) of the diffraction peaks of samples *A* and *B*. The $K\alpha_2$ component of the peaks was stripped from the data by appropriate software, and slow scans taken over all peaks well into the wings. The diffraction patterns are fit well assuming cubic material, which simplifies the analysis. A comparison of diffraction peaks for the typical (220) reflection, samples *A* and *B*, is shown in Fig. 2. This figure illustrates that for the high angle reflections, which are particularly sensitive to lattice strains, the width of the peaks for our sample *A* significantly exceeds the width for sample *B*. The data are analyzed systematically using the Williamson-Hall relationship[17,18] given by the expression below

$$\Gamma \cos\theta = \frac{\lambda}{L} + 2\left(\frac{\Delta d}{d}\right)\sin\theta, \tag{1}$$

where Γ is the FWHM of twice the Bragg angle, L is the particle size, and the other symbols have the usual meaning for x-ray diffraction. By plotting $\Gamma\cos\theta$ versus $\sin\theta$, one obtains a linear relationship. The intercept may be used to determine the particle size and the slope determines the strain term $\Delta d/d$.

One must, however, account for the instrumental broadening of the diffractometer in such studies. One method which has been used is to use a LaB_6 standard material to calibrate the instrument. This material is thoroughly characterized by NIST and has negligible strain broadening. For some applications, the peak broadening due to particle size effects has been assumed to be negligible for LaB_6. However, in our application we found that the particle size broadening of the LaB_6 diffraction peaks could not be neglected relative to the broadening of the diffraction peaks of samples *A* and *B*. The sizes of the crystallites in LaB_6 range from 2 to 5 μm,[19] as measured by NIST using a scanning electron microscope (SEM). By comparison, Potrepka *et al.* have made SEM estimates of sample grain sizes corresponding to BST with differing concentrations of equal Ta and Y dopants.[2] In the case corresponding to our samples *A* and *B*, the average grain size for the 1600 °C sinter was approximately 2 μm and the grain size of the 1550 °C sinter roughly half this value.[2] These grain sizes are sufficiently large, and the consequent broadening sufficiently small, that the broadening introduced by both the diffractometer (instrumental) and the LaB_6 (inherent broadening due to particle size) in a LaB_6 XRD scan can each be an appreciable fraction of the total peak broadening of samples *A* and *B*. In our case merely subtracting LaB_6 peak widths from experimental widths could result in an overcorrection for the instrumental broadening effect. However, something can be learned from the slope of a plot, if not the intercept, of the difference between the widths of the samples and the LaB_6 standard, since the strain broadening of LaB_6 is negligible. Using slope values of the linear fits from such a graph, the strain term $(\Delta d/d)$ was determined separately for samples *A* and *B*. These strains are 5.1×10^{-3} and 2.2×10^{-3}, respectively.

We further devised a modified version of the Williamson Hall plot appropriate to this situation. Let Γ_A be the FWHM of a peak corresponding to sample *A* and Γ_B be the corresponding width for sample *B*. L_A and L_B are the particle size of samples *A* and *B*, respectively. For any particular angle the instrumental contribution will be the same for both Γ_A and Γ_B and therefore one can plot the relationship shown below

$$(\Gamma_A - \Gamma_B)\cos\theta = \lambda\left(\frac{1}{L_A} - \frac{1}{L_B}\right) + 2\left[\left(\frac{\Delta d}{d}\right)_A - \left(\frac{\Delta d}{d}\right)_B\right]\sin\theta. \tag{2}$$

Relationship (2) above has the advantage that the instrumental contribution to the broadening is subtracted from the equation. One obtains the *difference* between the microstrain terms of the 1550 °C and 1600 °C sintered samples directly from the slope of a plot of $(\Gamma_A - \Gamma_B)\cos\theta$ versus $\sin\theta$. One can also test the grain sizes obtained, for consistency with the previously measured SEM results. Figure 3 shows a plot of Eq. (2), fit to a straight line by linear regression. From the intercept, and taking into account the standard error, we obtain the result given below

$$\left(\frac{1}{L_A} - \frac{1}{L_B}\right) = 1.9 \pm 1.3\ (\mu\text{m})^{-1}. \tag{3}$$

If we assume, from the SEM study of Potrepka *et al.*,[2] that L_B is roughly 2.0 μm, then the limits in Eq. (3) yield a value of L_A between 0.26 μm and 0.87 μm. These values are somewhat smaller than, but within a factor ~3, consistent with the values obtained by SEM for the 1550 °C sinter sample. The difference in strain between samples can be extracted directly from the slope of this curve and agrees with the difference between the strains of *A* and *B* given in the previous paragraph.

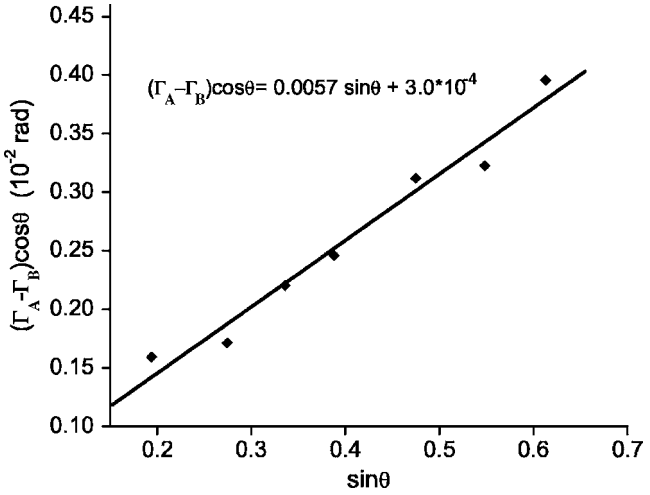

FIG. 3. A modified Williamson Hall plot of the difference between the broadening of samples *A* and *B* against sin θ. The linear fit for the data is shown by the solid line. The difference in the reciprocal of particle size, and the difference in the micro strain are estimated from the linear fit.

B. Ti *K*-edge XANES

The Ti *K*-edge XANES of $SrTiO_3$, BST, sample *A*, and sample *B* were obtained in fluorescence at room temperature. The data sets were normalized by standard methods, taking care to maintain the same energy range, normalization range, and spline range for all samples analyzed. The normalized XANES are illustrated in Fig. 4. In Fig. 4 we show an enlargement of the pre-edge region for these data, including all three newly measured samples plus existing data for $BaTiO_3$ and $EuTiO_3$.[20] The region between approximately 4968.5 eV and 4971.5 eV encompasses a peak labeled *X*, known to correspond to a *p* admixed final state that arises from hybridization between Ti 3*d* and O 2*p* orbitals. This hybridization results from displacement of the Ti atom from the centrosymmetric position within the oxygen octahedron.[21,22] Vedrinskii *et al.* have shown that a contribution to the area under peak *X* is given by Eq. (4) below

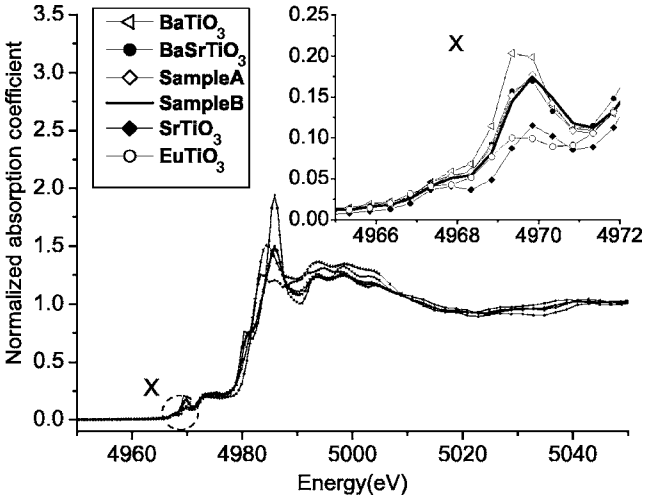

FIG. 4. Normalized XANES spectra of Ti *K* edge in $BaSrTiO_3$, samples *A* and *B*, and $SrTiO_3$. The data for bulk $BaTiO_3$ and a sample of $EuTiO_3$ are given for comparison. The feature *X* denotes the energy region of the dipole forbidden, $1s-3d$ transition. The insert shows the blow up region of $1s-3d$ transition. The vertical scale is in relative units.

$$A = \left(\frac{\gamma_s}{3}\right) d_s^2. \tag{4}$$

In this equation, d_S is off center Ti displacement and *A* is a peak area.[21] An experimental determination of the constant γ_S by Ravel resulted in values of 11.2 eV/A^2 for $BaTiO_3$ and 13.6 eV/A^2 for $EuTiO_3$,[20] with an error bar of about ± 3 eV/A^2. It is clear from Fig. 4 that, qualitatively, the Ti displacement is largest for $BaTiO_3$, smaller and essentially the same for BST, sample *A*, and sample *B*, and is significantly less for $SrTiO_3$ and $EuTiO_3$. We made use of the results of a recent study by Shuvaeva *et al.* who utilized the Ba L_3 EXAFS to study the Ti displacement from centrosymmetry in BST, and found that the displacement of Ti in BST is intermediate between that of $BaTiO_3$ and $SrTiO_3$.[23] We therefore assume an intermediate γ_S of 12.4 eV/A^2 for the BST materials. For $EuTiO_3$ there is no static Ti displacement, but a small displacement because of thermal vibrations.[20] Unstrained $SrTiO_3$ is not ferroelectric at any temperature,[24] and we assume the γ_S value for $SrTiO_3$ to be the same as $EuTiO_3$. These assignments of γ_S are rather arbitrary. However the inaccuracies involved do not change the basic conclusion from Fig. 4. This conclusion is that, for the Ta/Y doped BST materials, there is negligible influence of Ta/Y doping or sintering temperature on the average off center displacement of Ti from the octahedral center of inversion. We measured areas under the spectral peaks between the 4968 eV and 4971 eV energies by a similar method for all samples. Then the peak area of $EuTiO_3$ in the same energy region was subtracted. The assumption is made that the small peak in $EuTiO_3$ is entirely due to thermal vibration. Thus, in our procedure, the thermal vibration component is subtracted, so that only the static displacement contribution remains. For calculating the area under spectral peak of $EuTiO_3$, the experimentally measured values d_S=0.103 Å at 300 K and γ_S=13.6±3 eV/A^2 were used.[20] Figure 5 shows the measured static Ti displacements.

Our measured Ti displacement in undoped BST is intermediate between that of $BaTiO_3$ and $EuTiO_3$, in agreement with the recent study by Shuvaeva *et al.* These results all add credence to the main conclusion of our Ti *K*-edge study; which is that neither Ta/Y doping into BST nor sintering temperature affects the average Ti displacement, within experimental error. We therefore eliminate differences in average Ti displacement between samples as accounting for the observation that sample *A* exhibits relaxor behavior and sample *B* does not.

C. Ta and Y x-ray absorption edge fine structure data

The L_3 extended x-ray absorption edge fine structure (EXAFS) data for the Ta sites in *A* and *B* were obtained at beam lines X-11B of the NSLS. Si(111) monochromator crystals were used. The spectra were measured in the fluo-

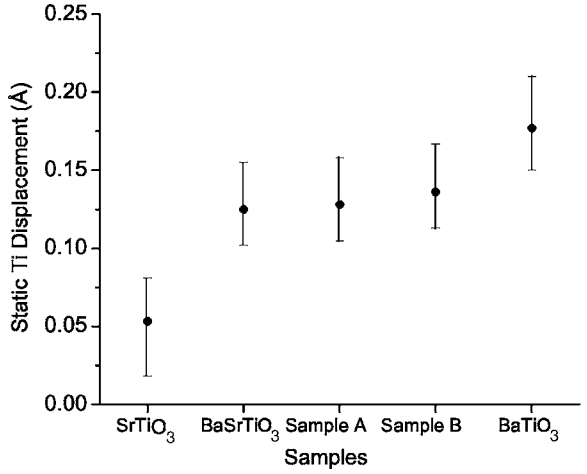

FIG. 5. A plot of the measured static Ti displacements of $BaSrTiO_3$, samples *A* and *B*, $BaTiO_3$ and $SrTiO_3$ is given including error bars.

rescence mode using an ion chamber filled with argon counting gas. Three reproducible spectra were obtained for each sample, aligned, and averaged. For the Ta and Y edges, the data were processed using the Artemis and Athena software packages, and background subtraction was carried out using the AUTOBK code.[25] These programs also enable one to normalize the absorption coefficient $\mu(k)$, and separate the oscillatory EXAFS, $\chi(k)$, from the absorption background. All three data sets were normalized and merged using the same k range $k=2$ to 13 Å^{-1}, k weighting of 2 and a hanning k window, for both samples *A* and *B*. Figure 6 shows a comparison of the normalized XANES, Fig. 7 shows the corresponding χ functions (background removed), and Fig. 8 shows the magnitude of the k^2 weighted Fourier transform corresponding to the k range 2.5 to 12 Å^{-1} in Fig. 7.

For the Y edges, twenty scans were normalized and averaged. Figure 9 shows the comparison of normalized XANES. Figure 10 shows the corresponding $\chi(k)$ functions.

Figure 11 shows the magnitude of the k^2 weighted Fourier transform corresponding to the $k=2$ to 15 Å^{-1} range in Fig. 10.

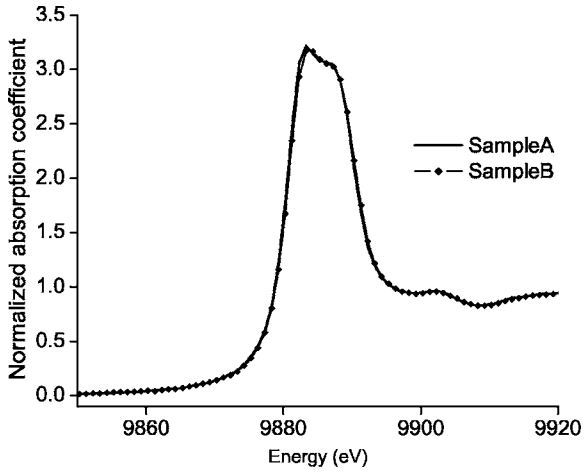

FIG. 6. Ta L_3-edge XANES: background removed and edge step normalized in samples *A* and *B*.

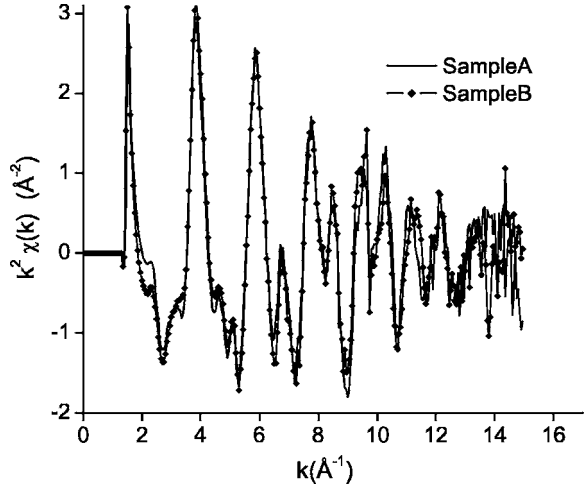

FIG. 7. Ta L_3-edge EXAFS: Background subtracted and edge step normalized $k^2\chi k$ in samples *A* and *B*.

The most striking aspect of the data is that, although there are no obvious differences in the Ta XAFS or FT for samples *A* and *B*, the Y XAFS and FT are quite different between these samples. Figure 11 shows that the main Fourier transform (FT) peaks of the EXAFS for sample *B* (1600 °C sinter) are significantly diminished relative to the FT peaks for sample *A* (1550 °C sinter). We suspect that some Y atoms have left the perovskite structure in sample *B*, and that therefore a simple perovskite model for analyzing the XAFS of *B* is not appropriate.

D. Data analysis

1. Fits for 1550 °C *sinter sample*

We fit the Ta L_3 and Y *K*-edge data of sample *A* simultaneously. We considered a model which contains for the third shell a mixture of Ta and Ti for Y centered spectra, and Y and Ti for Ta centered spectra. We imposed the constraint that the number of Ta third shell neighbors to Y equals the number of Y third shell neighbors to Ta. Also, the Debye-Waller term

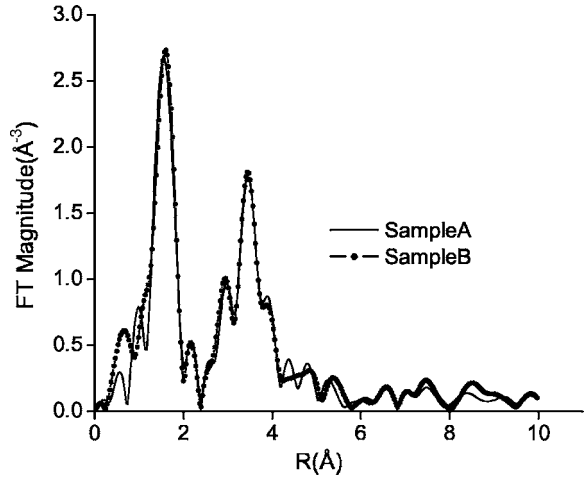

FIG. 8. Ta L_3-edge EXAFS: Fourier transform of $k^2\chi k$ in samples *A* and *B*.

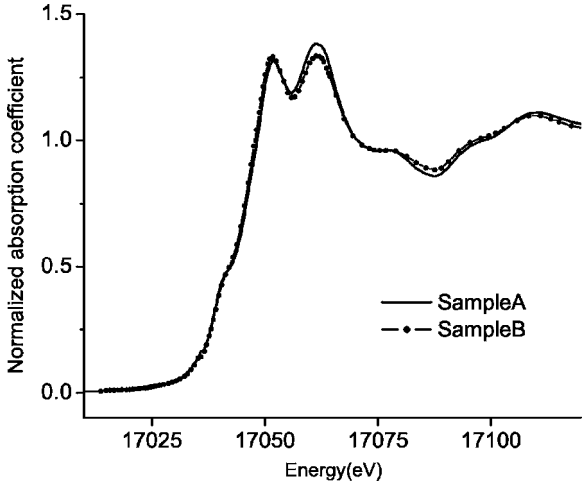

FIG. 9. Y *K*-edge XANES: Background subtracted and edge step normalized in samples *A* and *B*.

and the distances for Ta-Y and Y-Ta scattering paths were constrained to be the same. We assume a cubic perovskite structure. We have included best fit single scattering paths of first neighbor O and second neighbor Ba and Sr scatterers. We allowed different Debye-Waller terms for each of these paths. Also, we included single scattering (SS), double scattering (DS), and triple scattering (TS) paths for third shell Ti neighbors. For these three classes of paths we chose Debye-Waller factors with constraints (see the Appendix). The number of parameters varied in the fit was less than the number of independent data points. The distance from the central atom for this fit was in the range from 0.8 to 4.4 Å. The *R* factor for this fit was 0.0283 (Fig. 12). For optimum fit one obtains for the Ta atom that 98% of third shell neighbors are Ti and 2% Y, and for the Y atom that 98% of the third shell atoms are Ti and 2% Ta. However, our error bar for the percentage of clustered atom (Y or Ta) is ±13%. According to the calculations of Crowne, one would expect there to be only small clustering—a 17% chance of a Ta atom around each Y.[26] This prediction is barely outside our error bar.

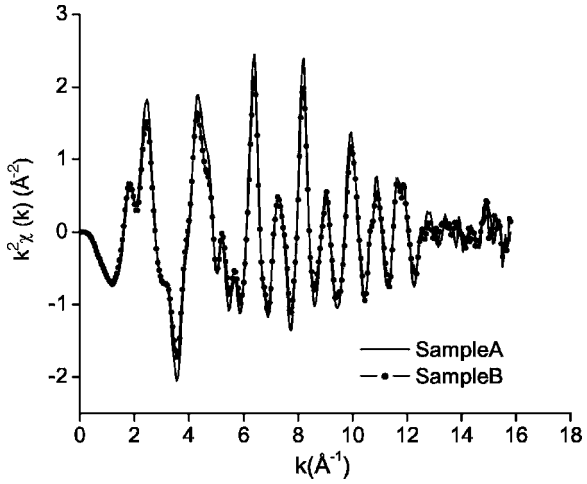

FIG. 10. Y *K*-edge EXAFS: Background subtracted and edge step normalized $k^2\chi k$ in samples *A* and *B*.

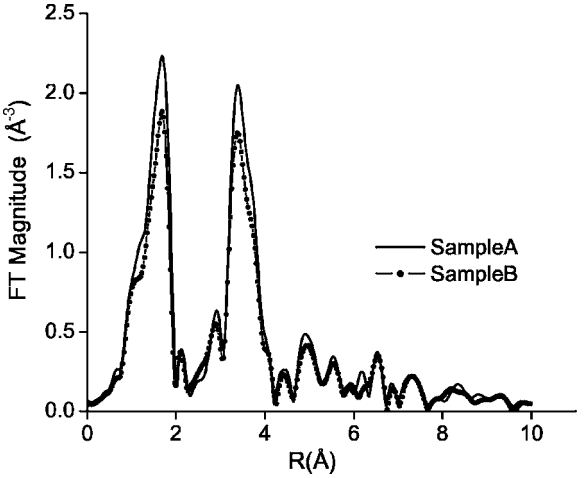

FIG. 11. Y *K*-edge EXAFS: Fourier transform of $k^2\chi k$ in samples *A* and *B*.

We note that the Ta-O bond lengths obtained from our fits are significantly less than expected based on the average crystal structure and all the Y centered bond lengths, other than Y-Ta, are significantly greater than expectations based on the average crystal structure (Table I). The BST crystallographic lattice constant we obtain from XRD is 3.972 Å, intermediate between the established value of 4.03 Å for $BaTiO_3$ and 3.91 Å for $SrTiO_3$. One might expect, therefore, Ta-O and Y-O bond lengths from EXAFS to be approximately half this intermediate value, or 1.986 Å. In fact, we obtain for our Ta-O and Y-O bond lengths, best fit values of 1.959 Å and 2.181 Å, respectively. The Y-O band is therefore longer than expected on the basis of the simple model and the Ta-O bond is shorter. Shannon estimates that the ionic radius of Y^{+3} ion in sixfold coordination indeed exceeds the ionic radius of Ta^{+5} ions in sixfold coordination by

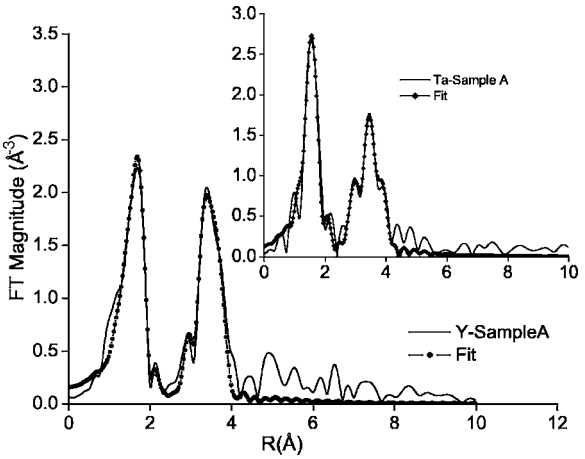

FIG. 12. This fit result is obtained by fitting Y *K*-edge and Ta L_3-edge EXAFS of sample *A* simultaneously, and the fit range is R=0.8 to 4.4 Å. We show the Fourier transform magnitude of the Y *K*-edge EXAFS in sample *A* and fit of theory model which contains for the third shell mixture of Ti and Ta around the Y atom. The insert shows the Fourier transform Ta L_3-edge EXAFS in sample *A* and fit of theory model which contains for the third shell mixture of Ti and Y around the Ta atom.

TABLE I. The best fit values for the nearest neighbor distances are shown. The Y *K*-edge and Ta L_3-edge data of sample *A* were fit with the model which contains for the third shell a mixture of Ta and Ti around Y atom and Ti and Y around Ta atom. The number(s) in the parentheses correspond to the uncertainty in the last digit(s) of the parameter.

Bond	Crystallographic bond length (theory) (Å)	Fit result *R* (Å)
Y-O	1.986	2.181(81)
Y-Ba	3.4399	3.543(18)
Y-Ti	3.9720	4.035(14)
Y-Sr	3.4399	3.568(22)
Y-Ta	3.9720	3.961(52)
Ta-O	1.986	1.959(16)
Ta-Ba	3.4399	3.392(71)
Ta-Ti	3.972	4.009(25)
Ta-Sr	3.4399	3.383(56)
Ta-Y	3.972	3.961(52)

a factor of 1.4.[27] The ratio of our Y-O to Ta-O distances in this system is actually less drastic than this estimate, and is only 1.1.

2. *Fits for* 1600 °C *sinter sample*

We fit the Ta edges of the 1600 °C sinter sample with a model that postulates only Ti in the third shell. An *R* factor of 0.0141 was obtained, which is the best *R* factor of all our fits. Here the tendency of the Ta centered bond lengths is to be closer to the crystallographically accepted values than for the fit to Ta edges of the 1550 °C sinter sample, but the difference is small and is less than the combined error bars (Table II). We also fit the Y *K*-edge data of sample *B* with the above model. The *R* factor for this fit is 0.0387 and the best fit value for the Debye-Waller factors of Y-Ti scattering paths is 0.0064 (Fig. 13). We note that, whereas the substitutional model for Ta in sample *B* gives the best *R* factor (0.0141) the corresponding model for Y in sample *B* yields the worst *R* factor of all our fits (0.0387).

We suspect that there may be more than one type of Y site in sample *B*, and that at the higher temperature sinter, some

TABLE II. The best fit values for the nearest neighbor Ta distances of sample *B* are shown. These distances are compared to the values for Ta distances of sample *A* taken from Table I. The number(s) in the parentheses correspond to the uncertainty in the last digit(s) of the parameter.

Bond	Crystallographic length (theory) (Å)	Fit results (Å)	
		Sample *A*	Sample *B*
Ta-O	1.986	1.959(16)	1.972(67)
Ta-Ba	3.4399	3.392(71)	3.404(23)
Ta-Ti	3.972	4.009(25)	4.021(11)
Ta-Sr	3.4399	3.383(56)	3.391(21)

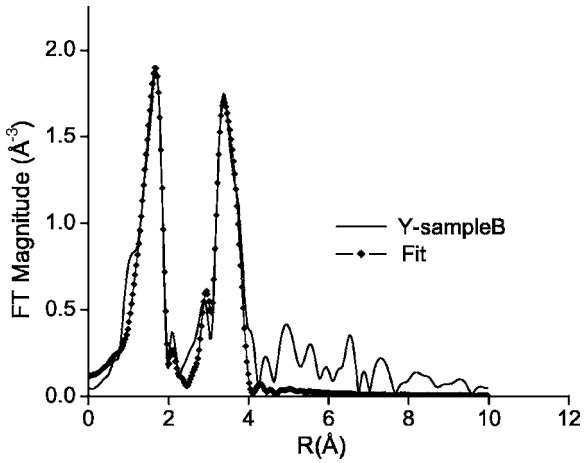

FIG. 13. FT magnitude of Y *K*-edge EXAFS of sample *B* and the fit of theory model which contains for the third shell pure Ti. The fitting *R* range is $R=0.8$ to 4.44 Å.

Y has left the perovskite lattice. Yttrium has an extremely high oxygen affinity, as will be discussed below. We have investigated an alternative model which compares the sample *B* yttrium XAFS, to a superposition of pure Y_2O_3 XAFS with sample *A* yttrium XAFS. There are obvious limitations to the validity of this description. For one thing, it is clear from the XRD results that the strain of the 1600 °C sinter sample is significantly less than the strain of the 1550 °C sample, although still large. If it were indeed the case that Y leaves the perovskite lattice to become Y_2O_3 in sample *B*, then the remaining perovskite is not really the same material as the perovskite in sample *A* and therefore this two site Y model is an approximation at best. We found that a combination of about 25% Y_2O_3 XAFS with 75% sample *A* Y edge XAFS yielded only a reasonable approximation to the sample *B* FT in Fig. 11, and we do not believe that we can uniquely determine the nature of the change in the Y environment between samples *A* and *B* using XAFS alone. We do note that there are several studies in the literature that find Y components of a system transforming to an oxide upon heat treatment. Choi *et al.* studied the crystallization of an amorphous $YMnO_3$ layer in a silicon substrate at 870 °C in oxygen.[28] A nanoscale Y_2O_3 layer formed between the $YMnO_3$ and the silicon substrate, as demonstrated by electron microscopy. The authors point out that the oxidizing ability of Y is about 2.4 times that of manganese, which is itself known as forming a quite stable oxide. Chengzhou *et al.* have studied Y implants in steel under high temperature oxidation.[29] Y_2O_3 forms readily due to the great difference between the heats of formation of Y_2O_3 (−153 kcal/g) versus Fe_2O_3 (−65.5 kcal/g). We observe no oxide peaks in either sample by XRD; however an informative test of these samples would be to chemically determine the bulk oxygen content of sample *B* versus *A*. However, only a truly bulk measurement is acceptable, since if extra oxygen atoms are entering sample *B* because of the higher temperature sinter, the composition could vary from surface to the bulk. The laboratory of one of us (Potrepka) is purchasing apparatus for combining wet chemical analysis with inductively

coupled plasma mass spectrometry. We intend to analyze our samples by these methods as a part of future studies.

IV. DISCUSSION

We have shed light on the nature of the relaxor sample *A*. We find no evidence that either the doping with Ta and Y or the different sintering temperatures modify the average Ti displacement from the center of the oxygen octahedron. However, we have shown that an outstanding difference between the relaxor type sample *A* and the normal ferroelectric *B* is that the internal stresses in sample *A* are significantly larger than in sample *B*. Before summarizing our other findings involving XAFS analysis, we will further discuss results relating to the internal stresses in such materials. Samara demonstrated pressure induced relaxor behavior in various compositionally disordered ferroelectrics.[30] Furthermore, Chaabane *et al.* have found a pressure induced suppression of diffuse scattering in a relaxor ferroelectric.[31] Studies by Soon *et al.* and Ang *et al.* are particularly germane to the present study. Soon *et al.* found that *A* site substitutions of Ba^{2+} and Sr^{2+} into $Pb_{0.7}La_{0.2}TiO_3$ generate tensile and compressive internal strains that are associated with relaxor behavior.[32] Ang *et al.* did not study internal strains, but have found that doping Ce into the Ti (*B* site) of $BaTiO_3$ produces a relaxor material.[33]

The microstrain in our sample *A* is large, given the small percentage of Ta and Y dopants. Noheda *et al.* have determined values of $(\Delta d/d)$ for a sample of $Pb(Zr_{0.52}Ti_{0.47})$ they have manufactured.[18] The measured strain value of this sample is 2.9×10^{-4} or about an order of magnitude less than the *difference* in the strains between our samples *A* and *B*. Balzar *et al.* have performed a recent theoretical-experimental study of the effect of inhomogeneous strain on the ferroelectric Curie temperature in thin films.[34] These samples had a strain of 2.5×10^{-3}. Again, this strain is comparable to the *difference* in the strains of our samples *A* and *B*, which are, furthermore, bulk samples and not subject to the strain from substrate stresses one can obtain in thin films. We note that the strain we determine for *B* site substitution of both Y^{3+} and Ta^{5+} into the 1550 °C sample of $[Ba_{0.6}Sr_{0.4}][(YTa)_{0.03}Ti_{0.94}]O_3$ is about half a percent. This strain is slightly greater than the maximum strain of 0.4% obtained by Soon *et al.* who doped (Ba^{2+}/Sr^{2+}) in the *A* site to produce (compressive/tensile) strains in $Pb_{0.7(1-x)}A_{0.7x}La_{0.2}TiO_3$.[31] Soon *et al.* attain a maximum strain for a value of $x=0.5$ whereas our samples have a larger strain than this at doping levels of Y and Ta of only 3% of the *B* sites. It is interesting that our sample *B* with a strain of 2.2×10^{-3} is a normal ferroelectric, but sample *A* with a strain only slightly more than twice this value is a relaxor. We note that the c/a ratio of pure ferroelectric $BaTiO_3$ only differs from unity by 1%,[15] and speculate that at a threshold value of microstrain, our system may transform from ferroelectric to relaxor.

A conclusion from the XAFS study is that whereas there are no striking differences between the environment of the Ta atoms in sample *A* versus sample *B*, there are large differences between the Y edges of these two samples. For the 1550 °C sinter sample, the XAFS results can be successfully modeled assuming Ta or Y substitution for Ti in the perovskite lattice; however, the Ta-O bonds are shorter than expected from the crystallography and the Y bonds longer. Our finding of longer Y centered bonds is consistent with the study of Y doped BST thin films by Ven Wang *et al.*, who find an expansion of the unit cell volume after Y doping to Ti sites.[35] There are investigations of various substances that imply that such deviations of local bonds from the crystallographically expected length can give rise to a distorted, even buckled structure.[36,37] It is likely that our perovskite structure with Ta or Y inclusions is also distorted.

We consider once again our XRD peak broadening study and the SEM results of Potrepka *et al.* These results are consistent with grain sizes in the 0.3 micron to 2.0 micron range.[2] Arlt *et al.* have found a correlation between grain size and ferroelectric domain width.[38] For $BaTiO_3$, these authors find that for grain sizes of 2 μm, the domain width is roughly 0.3 μm and for grain sizes of 0.5 μm the domain size is approximately 0.1 μm. In the model of Cross for relaxor behavior, the domain size is sufficiently small that that the polarization direction of a domain can be changed by thermal energies.[12] Different domain sizes will have differing Curie temperatures, which gives a relaxorlike behavior. These domain sizes are estimated by Cross to be of order 100 Å or less, which is at least one order of magnitude smaller than the estimate obtained from our XRD or SEM grain size estimates and the results of Arlt *et al.* On the other hand, Frey and Payne list several studies indicating that the critical size for loss of low temperature tetragonal distortion in pure $BaTiO_3$ may be as large as 0.1 μm.[9] However, we do not observe any difference in off center Ti displacement between the larger grained sample *B* and smaller grained sample *A*, which may have grain sizes on the order of 0.3 μm or larger. We believe that the grain sizes in our sample *A* are large enough to cast doubt on the Cross model for the relaxor behavior of this material. Although our XAFS studies show no tendency for clustering of Y and Ta pairs on the nanoscale, the error bars are large enough that the model of Cross cannot be ruled out.[12] We do believe that the large internal strains we observe in sample *A* must be an important component in any explanation of its relaxor behavior.

ACKNOWLEDGMENTS

We are grateful for the effort and support of the staff of the X-11B line of the National Synchrotron Light Source and the PNC-CAT line of the Advanced Photon Source. The present research was supported by the Department of Energy, Grant No. DE-FGO2-05ER36184. In addition, PNC-XOR facilities at the Advanced Photon Source, and research at these facilities, are supported by the U.S. DOE Office of Science Grant No. DEFG03-97ER45628, the University of Washington, a major facilities access grant from NSERC, Simon Fraser University, and the Advanced Photon Source. Use of the Advanced Photon Source is also supported by the U.S. Department of Energy, Office of Science, Office of Basic Energy Sciences, under Contract No. W-31-109-Eng-38. Research carried out at the National Synchrotron Light

Source, Brookhaven National Laboratory, is supported by the U.S. Department of Energy, Division of Materials Sciences and Division of Chemical Sciences, under Contract No. DE-AC02-98CH10886.

APPENDIX: EXAFS DEBYE-WALLER FACTORS OF COLLINEAR MULTIPLE-SCATTERING PATHS

For a multiple scattering photoelectron path originating from the absorbing atom, each leg of the path connecting instantaneous atomic positions is given by the vector: $\vec{r}_{ii+} = \vec{R}_{ii+} + \vec{u}_{i+} - \vec{u}_i$, where, following the notation of Poiarkova and Rehr,[39] $i+$ indicates the next nearest neighbor atom to i in the direction of the path, and $\vec{R}_{ii+}$ and $\vec{u}_i$ correspond to the average leg vector and atomic displacement vector, respectively. EXAFS Debye-Waller factor is defined as:

$$\sigma_j^2 \equiv \langle (r_j - R_j)^2 \rangle = \left\langle \left(\frac{1}{2} \sum_{i=1}^{n_j} (\vec{u}_i - \vec{u}_{i+}) \hat{R}_{ii+} \right)^2 \right\rangle = \frac{1}{4} \left\langle \left(\sum_{i=1}^{n_j} (\vec{u}_i - \vec{u}_{i+}) \hat{R}_{ii+} \right)^2 \right\rangle,$$

where $\hat{R}_{ii+}$ is the unit vector in the direction of $\vec{R}_{ii+}$. We now consider collinear paths from the central (absorbing) atom a to the atom c, where the average positions of atoms a, c, and the intervening atom b are on the same line. The corresponding DWFs of the single-scattering (SS) a-c-a, double-scattering (DS) a-b-c-a and the triple-scattering (TS) a-b-c-b-a collinear paths through intervening atom (b) are as follows:

$$\sigma_{\mathrm{TS}}^2 = \sigma_{\mathrm{DS}}^2 = \sigma_{\mathrm{SS}}^2 = \langle [(\vec{u}_a - \vec{u}_c)\hat{R}_0]^2 \rangle = \langle u_{ax}^2 \rangle + \langle u_{cx}^2 \rangle - 2\langle u_{ax} u_{cx} \rangle,$$

where $\hat{R}_0$ is the unit vector in the direction of the line connecting average positions of a and c, and the subscript x indicates x-component (along the line containing the atoms) of the displacement vector.

These relationships are modified if the central atom (a) is between two nearest neighbors (b and c), all three atoms having their average positions located on the same line. In that case, as in the equation above, the DWF of the SS path a-c-a is:

$$\sigma_{\mathrm{SS}}^2 = \langle u_{ax}^2 \rangle + \langle u_{cx}^2 \rangle - 2\langle u_{ax} u_{cx} \rangle.$$

The DWFs for the DS path (a-c-b-a) and TS paths (a-c-a-b-a) are equal to each other but not related to the 1NN SS:

$$\sigma_{\mathrm{TS}}^2 = \sigma_{\mathrm{DS}}^2 = \langle u_{bx}^2 \rangle + \langle u_{cx}^2 \rangle - 2\langle u_{bx} u_{cx} \rangle.$$

Finally, for the TS path a-c-a-c-a connecting the central atom and its nearest neighbor **c**, the DWF is equal to:

$$\sigma_{\mathrm{TS}}^2 = 4\sigma_{\mathrm{SS}}^2.$$

[1] D. M. Potrepka, S. C. Tidrow, and A. Tauber, Integr. Ferroelectr. **42**, 97 (2002).
[2] D. M. Potrepka, S. C. Tidrow, and A. Tauber, Mater. Res. Soc. Symp. Proc. **656**, E, DD5.9.1 (2001).
[3] J. R. Giniewicz, A. S. Bhalla, and L. E. Cross, Ferroelectr., Lett. Sect. **12**, 35 (1990).
[4] S. K. Streiffer, C. Basceri, C. B. Parker, S. E. Lash, and A. I. Kingon, J. Appl. Phys. **86**, 4565 (1999).
[5] T. Kawahara, M. Yamamuka, T. Makita, J. Naka, A. Yuuki, N. Mikami, and K. Ono, Jpn. J. Appl. Phys., Part 1 **33**, 5129 (1994).
[6] V. V. Lemanov, E. P. Smirnova, P. P. Syrnikov, and E. A. Tarakanov, Phys. Rev. B **54**, 3151 (1996).
[7] N. Sicron, B. Ravel, Y. Yacoby, E. A. Stern, F. Dogan, and J. J. Rehr, Phys. Rev. B **50**, 13168 (1994).
[8] R. Comes, M. Lambert, and A. Guinier, Solid State Commun. **6**, 715 (1968).
[9] M. H. Frey and D. A. Payne, Phys. Rev. B **54**, 3158 (1996).
[10] F. Crowne, S. C. Tidrow, D. M. Potrepka, and A. Tauber, Mater. Res. Soc. Symp. Proc. **720**, H6.5.1 (2002).
[11] G. A. Smolenskii, G. A. Isupov, V. A. Agrranouskaya, and N. Popov, Sov. Phys. Solid State **2**, 2584 (1961).
[12] L. E. Cross, Ferroelectrics **76**, 241 (1987).
[13] D. Viehland, S. J. Jang, L. E. Cross, and M. Wuttig, J. Appl. Phys. **68**(6), 2916 (1990).
[14] V. Westphal, W. Kleemann, and M. D. Glinchuk, Phys. Rev. Lett. **68**, 847 (1992).
[15] R. E. Cohen and H. Krakauer, Phys. Rev. B **42**, 6416 (1990).
[16] S. Heald (private communication).
[17] G. K. Williamson and W. H. Hall, Acta Metall. **1**, 22 (1953).
[18] B. Noheda, D. E. Cox, G. Shirane, J. A. Gonzalo, L. E. Cross, and S. E. Park, Appl. Phys. Lett. **74**, 2059 (1999).
[19] National Institute of Standards and Technology Certificate for Standard Reference Material 660a.
[20] B. Ravel, Ph.D. Thesis, University of Washington, 1995; B. Ravel, E. A. Stern, R. V. Vedrinskii, and V. L. Kraizman, Ferroelectrics **206**, 407 (1998).
[21] R. V. Vedrinskii, V. L. Kraizman, A. A. Novakovich, Ph. V. Demekhin, and S. V. Urazhdin. J. Phys.: Condens. Matter **10**, 9561 (1998); V. L. Kraizman, A. A. Novakovich, R. V. Vedrinskii, and U. A. Timoshevskii, Physica B **208**, 35 (1995).
[22] B. Ravel and E. A. Stern, Physica B **208**, 316 (1995).
[23] V. Shuvaeva, Y. Azuma, K. Yagi, H. Terauchi, R. V. Vedrinski, V. Komarov, and H. Kasatani, Phys. Rev. B **62**, 2969 (2000).
[24] J. H. Haeni, P. Irvin, W. Chang, R. Uecker, P. Reiche, Y. L. Li, S. Choudhury, W. Tian, M. E. Hawley, B. Craigo, A. K. Tagantsev, X. Q. Pan, S. K. Strieffer, L. Q. Chen, S. W. Kirchoefer, J. Levy, and D. G. Schlom, Nature (London) **430**, 758 (2004).
[25] M. Newville, P. Livins, Y. Yacoby, J. J. Rehr, and E. A. Stern, Phys. Rev. B **47**, 14126 (1993).
[26] F. Crowne (private communication).
[27] R. E. D. Shannon, Acta Crystallogr. **32**, 751 (1976).
[28] J. H. Choi, J. Y. Lee, and Y. T. Kim, Appl. Phys. Lett. **77**, 4028 (2000).

[29] J. Chengzhou, W. Anming, and L. Huailin, Surf. Coat. Technol. **128**, 213 (1999).
[30] G. A. Samara, Phys. Rev. Lett. **77**, 314 (1996).
[31] B. Chaabane, J. Kreisel, B. Dkhil, P. Bouvier, and M. Mezouar, Phys. Rev. Lett. **90**, 257601 (2003).
[32] H. P. Soon, J. M. Xue, and J. Wang, 14th IEEE International Symposium on Applications of Ferroelectrics, ISAF04, 320 (2004).
[33] C. Ang, Z. Yu, and Z. Jing, Phys. Rev. B **61**, 957 (2000).
[34] D. Balzar, P. A. Ramakrishnan, and A. M. Hermann, Phys. Rev. B **70**, 092103 (2004).
[35] R. Ven Wang, P. Mclntyre, J. Baniecki, K. Nomura, T. Shioga, K. Kurihara, and M. Ishii, Appl. Phys. Lett. **87**, 192906 (2005).
[36] A. V. Kolobov, P. Fons, A. I. Frenkel, A. Ankudinov, J. Tominaga, and T. Uruga, Nat. Mater. **3**, 703 (2004).
[37] A. Frenkel, E. A. Stern, A. Voronel, M. Qian, and M. Newville, Phys. Rev. Lett. **71**, 3485 (1993).
[38] G. Arlt, D. Hennings, and G. de With, J. Appl. Phys. **58**, 1619 (1985).
[39] A. V. Poiarkova and J. J. Rehr, Phys. Rev. B **59**, 948 (1999).